Experimental study of the interaction between convective and elliptical instabilities

Guillaume Lavorel and Michael Le Bars[a)]
Institut de Recherche sur les Phénomènes Hors Équilibre, UMR 6594 CNRS and Aix-Marseille Universités, 49 rue F. Joliot Curie, BP 146, F-13384 Marseille Cedex 13, France

(Received 10 June 2010; accepted 27 September 2010; published online 1 November 2010)

The reciprocal influence of convective and elliptical instabilities is studied experimentally in an elliptically deformed rotating cylindrical shell with an imposed temperature at the inner cylinder using the centrifugal force to mimic a radial gravity field. When the temperature contrast is stabilizing, we observe that the elliptical instability can grow and that the heat flux scales as the inverse of the viscous boundary layer depth. When the temperature profile is destabilizing, we observe (i) that the elliptical instability can still grow on the established convective motions, (ii) that for the experimental range of parameters, its growth rate progressively decreases when the intensity of convection increases, and (iii) that the elliptical instability modifies the heat transfer when the viscous boundary layer is smaller than the thermal one. Scaling laws for both cases are derived analytically and validated experimentally. We conclude that in geophysical and astrophysical systems, thermal effects have to be taken into account when looking for inertial instabilities and that these inertial instabilities have to be taken into account when evaluating heat transfers.
 [doi:10.1063/1.3508946]

I. INTRODUCTION

It is known from the analysis of Kelvin[1] that rotating flows support inertial (or "Kelvin") waves, whose origin comes from the restoring effect of the Coriolis force. These waves are generally damped by viscosity, but they can persist when an external forcing is applied. For instance, the elliptical instability arises in elliptically deformed systems from the triadic resonance between two Kelvin waves and the deformation.[2] Such an instability could be excited in the liquid core of planets that are tidally deformed by close bodies, leading, for instance, to the generation or induction of a magnetic field.[3,4] The dynamics of the elliptical instability has been studied in detail, following the first experimental approach of Malkus,[5] but always in the isothermal case. However, thermal effects have a fundamental importance in the dynamics of planetary cores. Indeed, convective flows are expected to control heat transfers and dynamo processes in most planets, as, for instance, in the Earth (see Ref. 6 for a review). Convective instabilities in rapidly rotating systems are also closely interconnected with inertial waves. Indeed, recent studies (e.g., Refs. 7 and 8) show that the convective flow can be represented, depending on the value of the Prandtl number, by either a single inertial-wave mode or by a combination of several inertial-wave modes and is controlled or influenced by the effect of the Ekman boundary layer. Moreover, following the Proudman–Taylor constraint, convective flows in rapidly rotating systems are almost invariant along the axis of rotation.[9] Experimentally, Busse and Carrigan[10] reproduced these columns in a rapidly rotating system submitted to a destabilizing temperature contrast using the centrifugal force to mimic the planetary radial gravity. In the present paper, we investigate the reciprocal influence of the elliptical instability and thermal effects in a fluid contained in a rotating cylindrical shell by coupling in a single experiment the historical setups of Malkus[5] and Busse and Carrigan.[10] Note that in addition to the geophysical interests, our study could also be relevant in some industrial applications, for instance, in the domain of vortex control in the wake of aircraft wings by means of injection of heated or cooled air.[11]

Le Bars and Le Dizès[12] studied analytically the linear stability of a rotating flow in an elliptically deformed cylindrical shell with an imposed (stable or unstable) conductive temperature profile. In this case, the elliptical instability comes from the resonance of gravito-inertial waves. They concluded that the growth rate of the elliptical instability is a decreasing function of the Rayleigh number, Ra, which characterizes the intensity of convection, and that the growth rate surprisingly increases with the intensity of stratification. Nevertheless, Le Bars and Le Dizès[12] did not investigate the nonlinear processes of the elliptical instability, and their stability analysis always started from a simple elliptical and nonconvective rotating base flow. This paper thus aims at completing these first conclusions by a systematic experimental study. Our purpose is to answer the following three questions: (i) could the elliptical instability grow in the presence of established convective motions? (ii) How are the growth rate of the elliptical instability and the convective heat flux modified? (iii) What is the predominant mechanism at the planetary scales? Note that the same questions are addressed numerically in the ellipsoidal geometry in a companion paper by Cébron *et al.*[13]

This paper is organized as follows. In Sec. II, the setup and the experimental procedure are presented. In Sec. III, the influence of the convection on the growth of the elliptical

[a)]Electronic mail: lebars@irphe.univ-mrs.fr. FAX: +33-4-96-13-97-09.

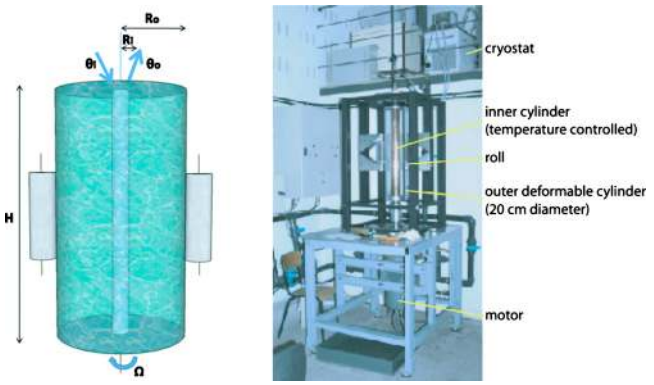

FIG. 1. (Color online) Sketch and picture of our experimental device. R_i and R_o designate the radii of the inner and the outer cylinders, respectively. H is the height of the tank and Ω is its rotation rate. θ_i and θ_o are the temperatures at the entrance and at the exit of the inner cylinder, respectively.

instability is studied experimentally. The experimental results regarding the influence of the elliptical instability on heat transfers are presented in Sec. IV, where general scaling laws are also derived. Finally, these scaling laws are applied to geo- and astrophysical systems in Sec. V.

II. EXPERIMENTAL SETUP

Our setup is a combination of the one developed by Busse and Carrigan[10] to study convective motions in a rapidly rotating system submitted to radial gravity and of the one developed by Malkus[5] to study the elliptical instability (see Fig. 1). A vertical cylindrical shell (height $H=80$ cm, inner radius $R_i=3$ cm, and outer radius $R_o=10$ cm) enclosed between two concentric cylinders is filled with water and set in rotation along the vertical axis at a constant angular velocity Ω, ranging from 150 to 350 rpm. This angular velocity is sufficiently rapid such that the local gravity is negligible compared to the centrifugal force.[9,10] We apply an elliptical deformation to the outer cylinder made of $e=3$ mm thick transparent polymethyl methacrylate (PMMA) by compressing it on its middle with two fixed vertical 20 cm long rollers aligned with the rotation axis. We measure the value s of the compression, which ranges between 0 and 4 mm. In the centrifugally driven case, the onset of convection is possible when the inner boundary is sufficiently cooled compared to the outer one. Otherwise, the flow is radially thermally stratified. In order to study both cases, we can either cool or heat the inner cylinder at a fixed temperature T_{in} by the circulation of a coolant fluid from a thermostated bath inside the inner cylinder, which is made of copper, so as to ensure an efficient heat transfer. Actually, the coolant fluid is injected in an inner pipe with a radius of 1 cm inside the copper cylinder from the top of the experiment. It flows through this pipe down to the bottom of the experiment and then goes back to the top through the outer circular ring inside the copper cylinder before being sucked. With this setup, we do not measure any temperature variation along the outer boundary of the copper cylinder. The top and bottom of our shell are made of 5 cm thick Plexiglas, ensuring a very good thermal isolation. Note that these flat ends are perpendicular to the axis of rotation. Four temperature probes (precisely calibrated thermocouples) permit to measure the inner and outer heat fluxes. Two probes measure the temperatures of the circulating fluid, respectively, at the entry θ_i and at the exit θ_o of the system. The mean inner heat flux is then given by

$$F_i = \frac{\rho c_p \Gamma(\theta_i - \theta_o)}{2\pi R_i H}, \tag{1}$$

where ρ is the density of the circulating fluid, c_p is its specific heat, and Γ is the flow rate of the thermostated bath measured via a flow meter. These two thermocouples also permit to define the surface temperature of the inner cylinder T_{in}, which we take as the mean value of θ_i and θ_o. Note that because of technical constraints, it was not possible to measure θ_i and θ_o exactly at the entrance of the inner cylinder. Corrections due to heat loss from the circulating pipe toward the surrounding atmosphere are thus included in F_i using a standard value of the heat transfer coefficient of the air. The local temperature at a given location of the inner surface of the outer cylinder T_i and the temperature of its outer surface T_o at the same location are measured by the two other probes. They permit one to define the local outer heat flux

$$F_o = k_p \frac{T_o - T_i}{e}, \tag{2}$$

where $k_p=0.2$ W m^{-1} K^{-1} is the thermal conductivity of the PMMA. We verified that once a thermal steady state is reached, the measured time-averaged values of the power through inner and outer cylinders ($2\pi R_i F_i H$ and $2\pi R_o F_o H$) are in good agreement, i.e., within 10%.

To visualize motions, we embedded the working fluid with anisotropic Kalliroscope flakes and used two separate systems of camera and laser sheet. In the first system, the laser and a wireless camera are embarked in rotation with the cylindrical shell, which allows one to visualize convective motions in a horizontal plane in the rotating frame. In the second system, a semirapid camera (200 frames/s) captures the dynamics of the elliptical instability from the laboratory frame through a vertical laser sheet, tangential to the inner cylinder.

According to the π-Buckingham theorem, six dimensionless parameters control the system. We choose

(a) the eccentricity of the outer cylinder measured at the midheight, $\epsilon = 2s/R_o$;
(b) the Ekman number based on the gap of the shell, $E = \nu/\Omega(R_o - R_i)^2$, where ν is the kinematic viscosity of the working fluid taken at the mean fluid temperature;
(c) the Rayleigh number based on the centrifugally gravity taken at the outer cylinder, $\text{Ra} = \alpha(T_i - T_{\text{in}})\Omega^2 R_o (R_o - R_i)^3/\kappa\nu$, where α is the thermal expansion coefficient of the working fluid and κ its thermal diffusivity;
(d) the thermal Prandtl number, $P = \nu/\kappa$;
(e) the shell aspect ratio, $a_1 = R_i/R_o$; and
(f) the cylinder aspect ratio, $a_2 = H/R_o$.

By systematically changing the temperature of the thermostated bath, the rotation rate, and the cylinder compression, we explored the following ranges: $\epsilon \in [0;0.08]$,

$E \in [5\times10^{-6};2\times10^{-5}]$, and $|\mathrm{Ra}| \in [10^7;10^9]$, with either a stabilizing (i.e., $\mathrm{Ra}<0$) or a destabilizing (i.e., $\mathrm{Ra}>0$) temperature contrast. The three other dimensionless parameters were kept constant, with the Prandtl number of water $P \approx 7.0$, the shell aspect ratio $a_1=0.30$, and a cylinder aspect ratio $a_2=8.0$, chosen so as to excite the isothermal principal mode $(-1,1,1)$ with an axial wavenumber equal to 2 in the notations of Eloy and Le Dizès[14] (i.e., the resonance between the Kelvin waves of azimuthal wavenumbers -1 and 1 with the simplest radial structure).

In our case, the critical Rayleigh number for the onset of the convection Ra_c is given by Busse and Carrigan[10] as

$$\mathrm{Ra}_c = 8\pi^2 E^{-1/2}\frac{\Delta R}{H}, \tag{3}$$

where $\Delta R=R_o-R_i$ is the size of the shell gap. This critical Rayleigh number corresponds to Eq. (2.13) of Ref. 10, where "the change in height can be neglected, the friction in the Ekman boundary layer becomes the dominant stabilizing force." It was derived in the small gap limit $\Delta R/R_o \ll 1$, which is not really fulfilled in our experiment. Nevertheless, we have not found in literature any analytical result for the critical Rayleigh number in the finite gap limit with an imposed temperature contrast, and we thus use this formula as a first order approximation. Note that since we do not change the value of ΔR and H in our study, the important point here is the dependence of Ra_c on $E^{-1/2}$, which we expect to be generic. The same dependence is indeed found in Ref. 15 in a geometry similar to our experimental setup but for convection induced by internal heating rather than by an imposed temperature contrast. Note also that our experimental device is not designed to evaluate the value of Ra_c and that a destabilizing temperature profile immediately leads to largely supercritical values of the Rayleigh number.

The same protocol was followed for all the experiments presented in this paper: (i) the system is set in rotation at a constant rate; (ii) after the spin-up time (at least 30 min), the inner cylinder is thermalized at the assigned constant temperature; (iii) once a thermal steady state is reached (after several hours), heat flow measurements for the reference nondeformed case are performed at the inner and outer cylinders; and finally (iv) the two rollers are pushed to deform elliptically the outer cylinder at the chosen eccentricity, and systematic measurements of heat flux as a function of the eccentricity are performed.

III. ON THE INFLUENCE OF THERMAL EFFECTS ON THE GROWTH OF THE ELLIPTICAL INSTABILITY

Here, we study, via systematic laboratory experiments, the potential development of the elliptical instability above the established convective motions. Using the embarked camera, we visualize the motions in the rotating frame in the presence of convection, with or without elliptical instability. A space-time diagram made along a radial line between the two cylinders and some corresponding snapshots are shown in Fig. 2. In the absence of outer cylinder compression, convective plumes (typical size: 1 cm) develop slowly and drift [Fig. 2(b)]. However, once a sufficient compression is applied, we observe cycles of rapid and fully turbulent small scale flows [Fig. 2(c)]. Snapshots of the evolution of the dynamics of the flow from the laboratory frame are presented in Fig. 3. The first snapshot [Fig. 3(a)] presents the flow before the deformation, with only convective motions. Vertical structures corresponding to convective columns are clearly visualized, whose trace in the horizontal plane corresponds to the plumes already described. Once the outer cylinder is deformed and if the deformation is sufficient, the effective axis of rotation of the fluid is progressively tilted, confirming the growth of the mode $(-1,1,1)$ of the elliptical instability above the established convective motions [Fig. 3(b)]. Its behavior is then similar to the cycling behavior observed in the isothermal case, as studied, for instance, by Eloy *et al.*[16] in the cylinder and by Herreman[17] in the cylindrical shell. After an exponential growth, the selected mode of instability saturates and finally explodes [Fig. 3(c)], giving rise to the small scale three-dimensional turbulence [Fig. 3(d)] also observed in the rotating frame. Finally, these small scales are dissipated by viscosity, the flow relaminarizes, and a new cycle starts [see also this cycling behavior in Fig.

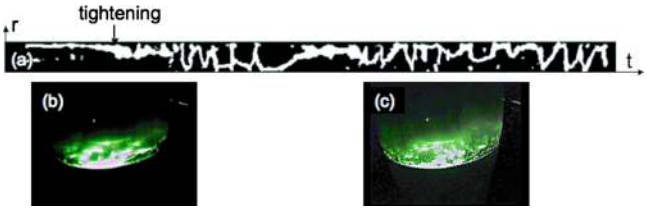

FIG. 2. (Color online) (a) Space-time diagram of the flow in the rotating frame made along a radial line of the cylindrical shell. The left part of the space-time diagram corresponds to the convective case in the absence of outer cylinder compression where the dynamics of the plumes is slow [see picture (b)], while the right part of the space-time diagram exhibits a more rapid and small scale chaotic dynamics, which takes place once a sufficient compression is applied [see picture (c)]. The dimensionless numbers are $\mathrm{Ra}=1.8\times10^8$, $E=6.4\times10^{-6}$, and $\epsilon=0.04$. See additional material online for a movie of the temporal evolution of the flow (enhanced online). [URL: http://dx.doi.org/10.1063/1.3508946.1]

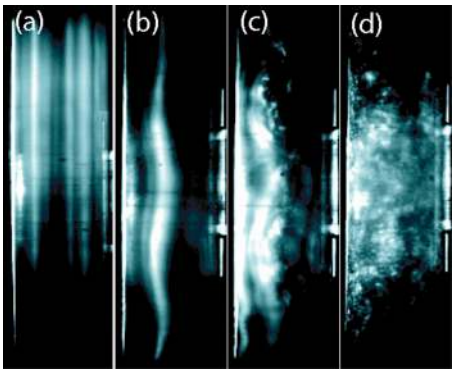

FIG. 3. (Color online) Four images extracted from a video sequence captured from the laboratory frame that show the growth of the mode $(-1,1,1)$ of the elliptical instability. (a) Time t=0: initial convective state, with vertical convective columns corresponding, in the horizontal plane, to Fig. 2(b). (b) t=1.5 s: growth of the mode. (c) t=3.5 s: saturation of the mode. (d) t=4 s: explosion that generates a three-dimensional turbulent flow corresponding, in the horizontal plane, to Fig. 2(c). This dynamics is cyclic. The dimensionless numbers are $\mathrm{Ra}=1.8\times10^8$, $E=6.4\times10^{-6}$, and $\epsilon=0.04$.

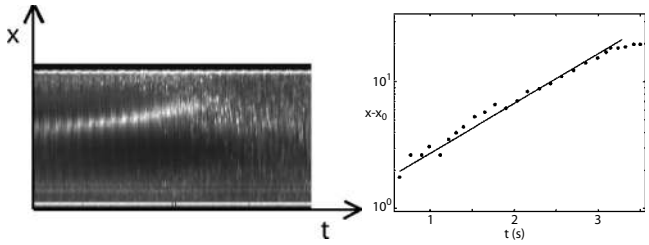

FIG. 4. Space-time diagram of the $(-1,1,1)$ mode, made along an horizontal line of a video sequence captured from the laboratory. The highlighted curve corresponds to the growth of the sinusoidal S shape of the mode, whose temporal evolution is reported on the right curve together with the best exponential fit, indicating the growth rate of the instability. The dimensionless numbers are $\mathrm{Ra}=1.6\times10^8$, $E=3.8\times10^{-6}$, and $\epsilon=0.06$.

2(a)]. As illustrated in Fig. 4, we measured the growth rate of the elliptical instability by extracting from the movie recorded in the laboratory frame, the maximum amplitude of the sinusoidal deformation of the rotation axis as visualized by Kalliroscope with respect to time. On the right curve in Fig. 4, the linear fit corresponding to the exponential growth of the instability before its nonlinear saturation is superimposed on the experimental measurements. The slope of this straight line gives a direct measurement of the linear growth rate σ of the instability. This measurement is difficult because of the great size of the device and of the large rotation rate, which induce very fast growth and relatively important vibrations. Nevertheless, we find that (i) in the absence of convection, our experimental results compare well with the asymptotic value of the dimensionless growth rate $\sigma=9\epsilon/16$ calculated for an unbounded, inviscid, and isothermal elliptical flow[2] and that (ii) the dimensionless growth rate σ is systematically smaller in the presence of convection. Figure 5 shows the evolution of the growth rate with the Rayleigh number for two values of the Ekman number E. We conclude that the convection has a stabilizing influence on the growth of the elliptical instability. In their linear study of the elliptical instability in the presence of a diffusive temperature profile, Le Bars and Le Dizès[12] concluded similarly on the stabilizing influence of an increasing Rayleigh number and quantified this influence. They predicted corrections in the growth rate and selected wave numbers of order $\widetilde{\mathrm{Ra}}=\alpha(T_i-T_{\mathrm{in}})/(\ln R_i/R_o)$. In our experiments, $\widetilde{\mathrm{Ra}}$ typically ranges between 2×10^{-4} and 5×10^{-3}, so this theoretically predicted dependence cannot explain the results presented in Fig. 5. Besides, we did not observe any change regarding the selected wave number when increasing the Rayleigh number. In fact, the significant variations of the growth rate measured experimentally must be related to the presence of an established convective flow that was not taken into account in the linear study. We can understand this effect qualitatively as a function of Ra by looking at the base flow above which the elliptical instability grows. For intermediate values of Ra (as those explored in the experiment), convective motions are two dimensional and take place at a typical scale comparable to the size of the gap. They can thus be considered as perturbations of the isothermal elliptical base flow at an intermediate scale. When the Rayleigh number increases, the streamlines are more and more disturbed compared to the isothermal elliptical ones so that the elliptical forcing is less and less felt by fluid particles and the growth rate of the tidal instability decreases. There might even exist a Rayleigh number above which the elliptical instability cannot grow. However, when further increasing Ra, the convection becomes fully turbulent and three dimensional, with very small scale eddies: it is then possible to define an eddy viscosity that replaces the kinematic viscosity. Thus, the elliptical in-

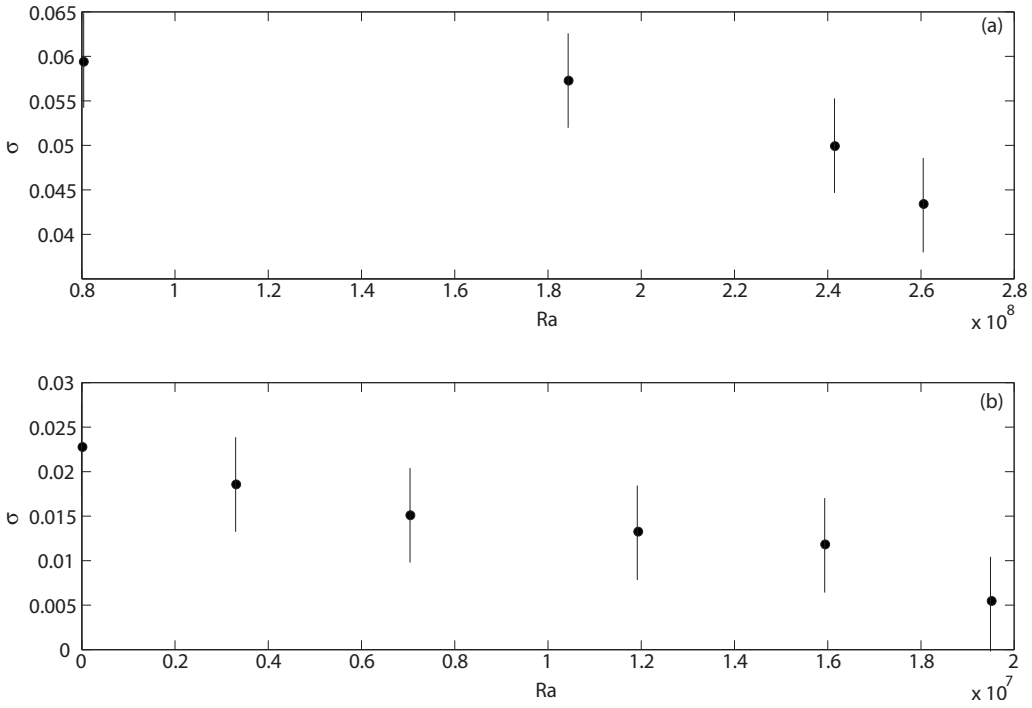

FIG. 5. Dimensionless growth rate σ as a function of Ra for $\epsilon=0.08$ and for (a) $E=9.7\times10^{-6}$ and (b) $E=3.9\times10^{-5}$.

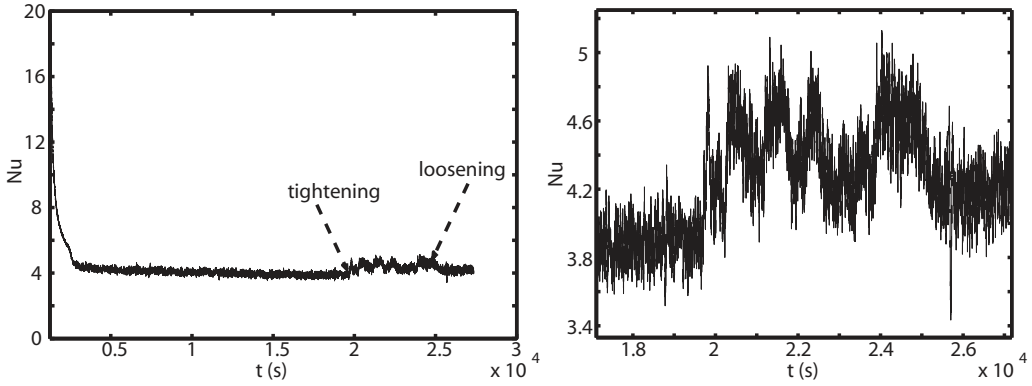

FIG. 6. Typical temporal evolution of Nu in a convective case for $\epsilon=0.06$, $\mathrm{Ra}=10^8$ (once the thermal equilibrium is reached), and $E=9.7\times10^{-6}$. A zoom on the elliptically unstable stage is made, with the presence of fluctuations linked to the dynamics of the instability.

stability should reappear, provided that the deformation is sufficient to overcome viscous diffusion using the turbulent (rather than molecular) viscosity. Note that the study of Fabijonas and Holm,[18] using the rotating Craik–Criminale solutions of the Lagrangian-averaged Navier-Stokes α turbulence model, even shows that three-dimensional turbulence enhances the inviscid growth rate of the elliptical instability for Kelvin wavelengths that are larger than the turbulence correlation length. The study of this peculiar fully turbulent regime is very interesting, but unfortunately, it is beyond the possibilities of our present experiment. We thus plan to tackle this limit in a future experiment using grid generated turbulence.

IV. ON THE INFLUENCE OF THE ELLIPTICAL INSTABILITY ON HEAT TRANSFERS

As we discussed in Sec. I, centrifugally driven convection is typically organized in convection columns parallel to the rotation axis. We also saw in Sec. III that this organization is completely broken in the presence of the elliptical instability. Here, we study, via our laboratory experiment, the influence of the changes of the flow due to the elliptical instability on the radial heat transfer.

To do so, we introduce the Nusselt dimensionless number, Nu, which characterizes the efficiency of the real heat transfer compared to the purely conductive heat transfer. In the case of a cylindrical shell, the diffusive heat transfer can be written as $2\pi k_e H\Delta T/\ln(R_o/R_i)$ and the Nusselt number is given by

$$\mathrm{Nu}=\frac{\text{total heat transfer}}{\text{conductive heat transfer}}=\frac{2\pi R_i H F_i}{2\pi k_e H\Delta T/\ln(R_o/R_i)}, \tag{4}$$

where k_e is the thermal conductivity of the working fluid, $\Delta T=|T_i-T_{\mathrm{in}}|$, and F_i is the inner flux defined in Sec. I. We use F_i to calculate Nu rather than the outer flux F_o because F_i is a mean value of the flux averaged over the whole inner cylinder, whereas F_o is measured locally at a given location of the outer cylinder. In Fig. 6, a typical temporal evolution of Nu for a convective case is shown. Once the thermal steady state is reached, the two lateral rollers are pushed on the outer cylinder, and if the deformation is sufficient, a mode of the elliptical instability grows and the Nusselt number increases. Then, the Nusselt number does not stay constant, but its fluctuations correspond to the observed hydrodynamic cycles. During the laminarization phase, Nu decreases, while during the turbulent stage, Nu increases. Once the elliptical constraint is released, Nu goes back to its value before the tidal deformation, provided that the thermal steady state is effectively reached.

Following the recent study of King *et al.*[19] regarding the two regimes of heat transfer in rotating Rayleigh–Bénard convection, the sudden variation of the heat flux can be explained by a boundary layer control. Indeed, our fluid volume schematically consists of three distinct regions: the interior of the fluid (the bulk) and two vertical boundary layers situated near the inner and outer cylinders. The boundary layers located at the top and at the bottom of the shell are not considered here because the heat flux is negligible there. The boundary layers are thin regions where heat transfer is controlled by diffusion, whereas the bulk is well-mixed and isothermal. So, the heat transfer is completely controlled by the thickness of the boundary layers δ and the inner heat flux scales as $F_i=k_e\Delta T_i/\delta$, and similarly for the outer heat flux. Here, ΔT_i is the temperature difference across the inner boundary layer and is given by the conservation of the total power $2\pi R_i F_i H=2\pi R_o F_o H$ plus the simple equation $\Delta T=\Delta T_i+\Delta T_o$, i.e., $\Delta T_i=\Delta T R_o/(R_o+R_i)$. The Nusselt number then scales as $\mathrm{Nu}=R_i R_o\ln(R_o/R_i)/\delta(R_i+R_o)$.

Considering the elliptical instability only, the vertical boundary layers are viscous layers of thickness δ_E, which scales like $\delta_E\sim\Delta R E_{\mathrm{EI}}^{1/2}$. Here, E_{EI} is the Ekman number based on the typical velocity of the elliptical instability. As shown numerically by Cébron *et al.*,[20] $E_{\mathrm{EI}}=E$, except in the vicinity of the threshold of the elliptical instability given by the critical Ekman number, $E_c\sim(\epsilon/5.24)^2$, where $E_{\mathrm{EI}}\sim E/\sqrt{E^{-1}-E_c^{-1}}$. Now, considering convective motions only, the boundary layers are thermal boundary layers of thickness δ_κ, which scales like $\delta_\kappa\sim\Delta R(\mathrm{Ra}/\mathrm{Ra}_c)^{-\beta}$, where β is a positive constant, such that the thermal boundary layers become thinner as the vigor of the convection increases. The numerical value of β depends of the type of convection we consider. For the classical Rayleigh–Bénard convection, $\beta=1/3$ is the most common scaling.[21] In our case with a cylindrical shell

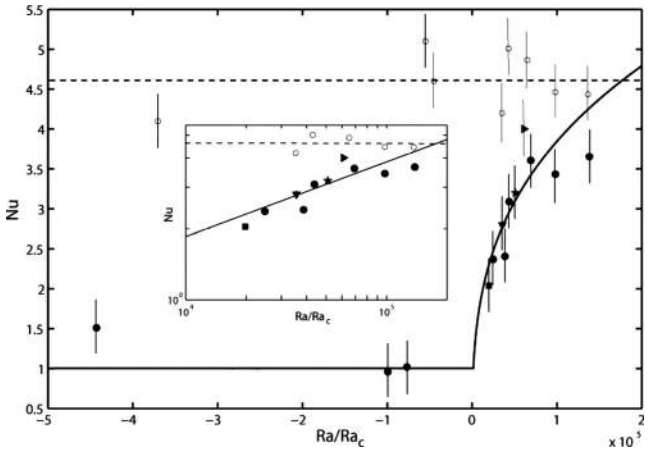

FIG. 7. Plot of the Nusselt number, Nu, as a function of the ratio between the Rayleigh number and the critical Rayleigh number, $\mathrm{Ra}/\mathrm{Ra}_c$, without (filled symbols) and with elliptical instability (empty symbols, $\epsilon=0.04$). Ra_c is calculated for different Ekman numbers following Busse and Carrigan (Ref. 10): $E=1.3\times10^{-5}$ (squares), $E=9.7\times10^{-6}$ (circles), $E=7.8\times10^{-6}$ (vertical triangles), $E=6.5\times10^{-6}$ (stars), and $E=5.6\times10^{-6}$ (horizontal triangles). The solid line represents the best fit for the convective case (i.e., $\mathrm{Ra}>\mathrm{Ra}_c$), giving the scaling law $\mathrm{Nu}=0.097(\mathrm{Ra}/\mathrm{Ra}_c)^{0.32}$ above the threshold and $\mathrm{Nu}=1$ otherwise. The dotted line represents the mean experimental value (i.e., $\mathrm{Nu}=4.6$) in the presence of the elliptical instability. A zoom on the convective part is presented in the inset with a logarithmic plot.

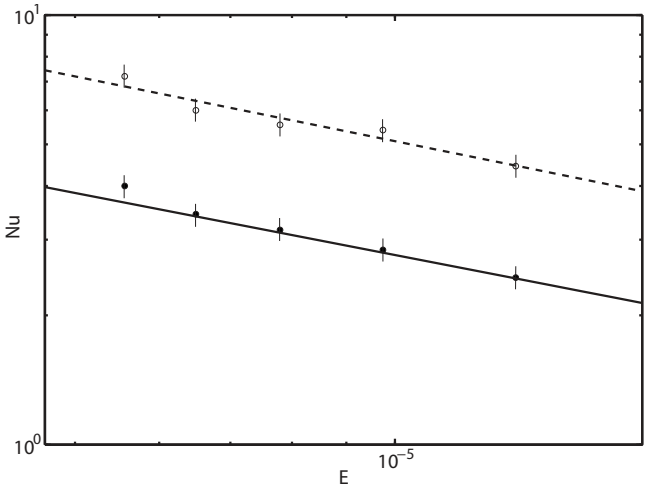

FIG. 8. Logarithmic plot of Nu as a function of E without (filled circles) and with elliptical instability (empty circles) for $\epsilon=0.04$ and $\Delta T=3$ K. The dashed line represents the best fit in the elliptically unstable case, $\mathrm{Nu}_E=0.016E^{-0.50}$. The continuous line corresponds to the scaling law determined in Fig. 7 for the purely thermal (elliptically stable) case.

and flat top and bottom perpendicular to the rotation axis, the same value is expected.

In our experiment, considering the convective structures as the base state above which the elliptical instability grows, there are two possible regimes: (i) the thermal boundary layers are thinner than the viscous layers, $\delta_\kappa<\delta_E$, so that the elliptical instability grows inside the convective bulk and (ii) the viscous layers are thinner than the thermal ones, $\delta_E<\delta_\kappa$, so that the elliptical instability also partially grows over the thermal boundary layers. The transition between "thermal-control" by the convection and "viscous-control" due to the elliptical instability occurs when $\delta_\kappa\approx\delta_E$, corresponding to a transitional Nusselt number, Nu_t. Our experiment allows us to change the thickness of the thermal boundary layers alone by varying the temperature contrast. The series of Nusselt number measurements for various Rayleigh and Ekman numbers are presented in Fig. 7 as a function of $\mathrm{Ra}/\mathrm{Ra}_c$, with and without elliptical instability. Note that in the experimental data, Ra_c is different for each Ekman number considered and computed according to Eq. (3). Concerning the elliptically stable but convectively unstable case, the best fit of the heat transfer data in terms of $\mathrm{Ra}/\mathrm{Ra}_c$ power law gives

$$\mathrm{Nu}=0.097\left(\frac{\mathrm{Ra}}{\mathrm{Ra}_c}\right)^{0.32}. \tag{5}$$

The obtained coefficient is consistent with the expected 1/3. When elliptical instability is included, heat transfer becomes larger for all studied cases, especially in the stratified case ($\mathrm{Ra}<0$), and the Nusselt number remains roughly constant equal to 4.6 when changing Ra. This behavior is compatible with a viscous rather than thermal boundary layer control. We define the transition between the thermal-control regime and the viscous-control regime as the point of intersection between their respective scalings, $\mathrm{Nu}=0.097(\mathrm{Ra}/\mathrm{Ra}_c)^{0.32}$ and $\mathrm{Nu}=4.6$. Equating the two, we solve for the transitional Rayleigh number,

$$\mathrm{Ra}_t=1.4\times10^7\frac{\Delta R}{H}E^{-1/2}. \tag{6}$$

When $\mathrm{Ra}<\mathrm{Ra}_t$, convection is not sufficiently strong and heat transfer is affected by the elliptical instability. When $\mathrm{Ra}>\mathrm{Ra}_t$, heat transfer is not affected by the elliptical instability and follows the convective scaling. For example in our experiment, $\mathrm{Ra}_t=3.9\times10^8$ when $E=9.7\times10^{-6}$. Unfortunately, our setup does not allow to reach such values.

We can also explore the dependence of the heat flux on the Ekman number by systematically changing the rotation rate in maintaining $\Omega^2R_o>g$ and ΔT constant. Note however that since our apparent gravity is related to the centrifugal force, changing the rotation rate also changes the Rayleigh number. In Fig. 8, the behavior of the heat transfer as a function of the Ekman number is shown, with and without elliptical instability. Concerning the elliptically unstable case, where the heat transfer is larger, the best fit of the heat transfer data gives the scaling law

$$\mathrm{Nu}_E=0.016E^{-0.50}. \tag{7}$$

The obtained exponent is in excellent agreement with the expected exponent $-1/2$, which validates the hypothesis of control by the viscous boundary layer. The prefactor is also in very good agreement with the results of Cébron *et al.*,[13] who determined a prefactor equal to 0.01 for a spherical shell. Concerning the elliptically stable case, expressing Eq. (5) in the configuration of constant ΔT and variable Ω leads to

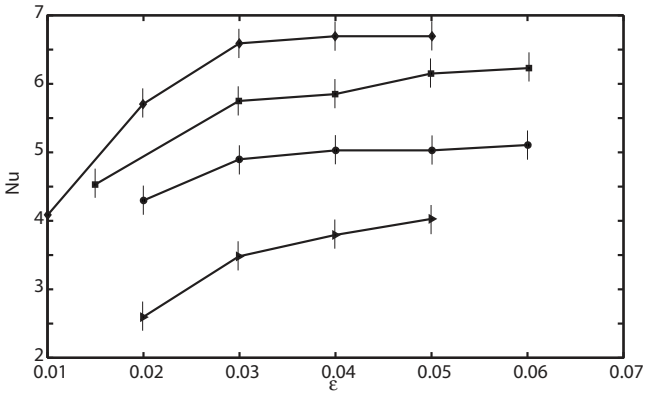

FIG. 9. Nu as a function of ϵ for different E. Triangles: $E=1.3\times10^{-5}$; circles: $E=9.7\times10^{-6}$; squares: $E=6.5\times10^{-6}$; and diamonds: $E=5.6\times10^{-6}$. Above the threshold of the elliptical instability, Nu changes with the amplitude of the instability following a typical supercritical bifurcation, until it rapidly saturates.

$$\mathrm{Nu}_\kappa = 0.097\left(\frac{\alpha\Delta T H R_o \nu}{8\pi^2\Delta R^2\kappa}\right)^{0.32} E^{-0.48}. \tag{8}$$

As shown in Fig. 8, the scaling closely agrees with our systematic experimental measurements.

Our last study concerns the dependence of Nu as a function of the eccentricity ϵ. In Fig. 9, this dependence is plotted for different E. We notice that in agreement with Eq. (7), Nu increases when E decreases. For each experiment at constant Ekman number, Nu increases close to the threshold of the elliptical instability and rapidly reaches a constant value at larger ϵ. This evolution is related to the evolution of E_{EI}, i.e., the Ekman number based on the typical velocity of the elliptical instability introduced before, which implies a scaling of Nu in $[E/\sqrt{E^{-1}-(5.24/\epsilon)^2}]^{-1/2}$ close to the threshold and a rapid saturation toward $E^{-1/2}$ once the deformation is sufficient. This result thus also validates our analysis in terms of the relative thickness of the two types of boundary layers.

To finish with, note that the recent study of Schmitz and Tilgner[22] has suggested an alternative explanation to King *et al.*[19] regarding the heat flux control of rotating Rayleigh–Bénard convection. Indeed, their numerical simulations also show the presence of two regimes as the function of the rotation rate even if their system has no Ekman layer. Hence, they do not interpret their results in terms of boundary layers competition, but rather in terms of advective flux competition in the bulk. In our case, the relevant advective heat flux in the bulk is related to the velocity along the imposed temperature gradient, which comes from the Ekman pumping induced by the elliptical instability. This Ekman pumping also scales in $E^{-1/2}$ and induces the same Nu scalings as those that we obtained with the boundary layer analysis. Hence, we cannot discriminate one or the other control mechanism.

V. CONCLUSION

This paper presents the first systematic experimental study of the reciprocal influence of the elliptical and convective instabilities in an elliptically deformed and differentially heated rotating cylindrical shell. The first predominant result is that the elliptical instability grows on the established convective motions even if its growth rate decreases when the intensity of the convection increases. We have also found scaling laws characterizing the Nusselt number. Two regimes were found corresponding to boundary layers controlled by either thermal dissipation or viscous diffusion. Even if the range of parameters (Ekman and Rayleigh numbers) accessible to our experimental device is relatively limited, we have identified and validated the general physical mechanisms that control the heat transfer, with or without elliptical instability.

In the Earth's core, convective motions are different from our case because of geometrical constrains. Indeed, they take the form of Busse columns[9] around the inner solid core, which propagate as thermal Rossby waves. Hence, scaling law for heat transfers is different. Christensen and Aubert[23] determined

$$\mathrm{Nu}-1 = 0.14\left(\frac{\mathrm{Ra}}{\mathrm{Ra}_c}\right)^{1.1}, \tag{9}$$

where Ra_c scales like $E^{-4/3}$.[24] A good way to reproduce this type of motions in the laboratory is to incline the top and bottom boundaries of the shell.[10] This will be the subject of a future study. However, we already expect the physical mechanisms shown here to remain valid. In particular, the scaling (7) is robust and should persist in planetary cases.[13] Equating this scaling with Eq. (9), we can evaluate the transitional Rayleigh number, Ra_t, as a function of E,

$$\mathrm{Ra}_t = \mathrm{Ra}_c\left(\frac{0.016E^{-0.50}-1}{0.14}\right)^{1/1.1}, \tag{10}$$

A typical estimation of the Ekman number in the Earth's liquid metal outer core is $E\approx10^{-15}$, which gives a transitional Rayleigh number, $\mathrm{Ra}_t\approx7.2\times10^{22}$. This result suggests that the outer Earth's core, where $\mathrm{Ra}\approx8\times10^{24}$,[23,25] is above the transition between the two regimes; hence, it is thermally controlled. Nevertheless, due to the closeness of the obtained values, a tidally dominated flux is not precluded in other convective planetary systems. Note also that the heat transfer by elliptical instability could be especially important in the outer stratified part of the core,[26] which should not be considered as a thermal blanket.

[1] Lord Kelvin, "Vibrations of a columnar vortex," Philos. Mag. **10**, 155 (1880).
[2] F. Waleffe, "On the three-dimensional instability of strained vortices," Phys. Fluids A **2**, 76 (1990).
[3] L. Lacaze, W. Herreman, M. Le Bars, S. Le Dizès, and P. Le Gal, "Magnetic field induced by elliptical instability in a rotating spheroid," Geophys. Astrophys. Fluid Dyn. **100**, 299 (2006).
[4] R. Kerswell and W. Malkus, "Tidal instability as the source for Io's magnetic signature," Geophys. Res. Lett. **25**, 603 (1998).
[5] W. Malkus, "An experimental study of global instabilities due to tidal (elliptical) distortion of a rotating elastic cylinder," Geophys. Astrophys. Fluid Dyn. **48**, 123 (1989).
[6] P. Roberts and G. Glatzmaier, "Geodynamo theory and simulations," Rev. Mod. Phys. **72**, 1081 (2000).
[7] K. Zhang, X. Liao, and F. H. Busse, "Asymptotic solutions of convection in rapidly rotating non-slip spheres," J. Fluid Mech. **578**, 371 (2007).
[8] K. Zhang and X. Liao, "The onset of convection in rotating circular cylinders with experimental boundary conditions," J. Fluid Mech. **622**, 63 (2009).

[9]F. H. Busse, "Thermal instabilities in rapidly rotating systems," J. Fluid Mech. **44**, 441 (1970).
[10]F. H. Busse and C. R. Carrigan, "Convection induced by centrifugal buoyancy," J. Fluid Mech. **62**, 579 (1974).
[11]D. Sipp, D. Fabre, S. Michelin, and L. Jacquin, "Stability of a vortex with a heavy core," J. Fluid Mech. **526**, 67 (2005).
[12]M. Le Bars and S. Le Dizès, "Thermo-elliptical instability in a rotating cylindrical shell," J. Fluid Mech. **563**, 189 (2006).
[13]D. Cébron, P. Maubert, and M. Le Bars, "Tidal instability in a rotating and differentially heated ellipsoidal shell," Geophys. J. Int. **182**, 1311 (2010).
[14]C. Eloy and S. Le Dizès, "Stability of the Rankine vortex in a multipolar strain field," Phys. Fluids **13**, 660 (2001).
[15]K. Zhang and G. T. Greed, "Convection in rotating annulus: An asymptotic theory and numerical solutions," Phys. Fluids **10**, 2396 (1998).
[16]C. Eloy, P. Le Gal, and S. Le Dizès, "Elliptic and triangular instabilities in rotating cylinders," J. Fluid Mech. **476**, 357 (2003).
[17]W. Herreman, "Instabilité elliptique sous champ magnétique et dynamo d'ondes inertielles," Ph.D. thesis, Université de Provence, 2009.
[18]B. Fabijonas and D. Holm, "Craik-Criminale solutions and elliptic instability in nonlinear-reactive closure models for turbulence," Phys. Fluids **16**, 853 (2004).
[19]E. King, S. Stellmach, J. Noir, U. Hansen, and J. Aurnou, "Boundary layer control of rotating convection systems," Nature (London) **457**, 301 (2009).
[20]D. Cébron, M. Le Bars, J. Leontini, P. Maubert, and P. Le Gal, "A systematic numerical study of the tidal instability in a rotating ellipsoid," Phys. Earth Planet. Inter. **182**, 119 (2010).
[21]L. Howard, "Convection at high Rayleigh number," in *Proceedings of the 11th International Congress on Applied Mechanics*, Münich, edited by H. Görtler (Springer-Verlag, Berlin, 1964), pp. 1109–1115.
[22]S. Schmitz and A. Tilgner, "Heat transport in rotating convection without Ekman layers," Phys. Rev. E **80**, 015305(R) (2009).
[23]U. Christensen and J. Aubert, "Scaling properties of convection-driven dynamos in rotating spherical shells and application to planetary magnetic fields," Geophys. J. Int. **166**, 97 (2006).
[24]C. R. Carrigan and F. H. Busse, "An experimental and theoretical investigation of the onset of convection in rotating spherical shells," J. Fluid Mech. **126**, 287 (1983).
[25]J. M. Aurnou, "Planetary core dynamics and convective heat transfer scaling," Geophys. Astrophys. Fluid Dyn. **101**, 327 (2007).
[26]R. Kerswell, "Elliptic instabilities of stratified, hydromagnetic waves," Geophys. Astrophys. Fluid Dyn. **71**, 105 (1993).